Thermal Analysis of Duplex 3-Phase Induction Motor Under Fault Operating Conditions

M. Popescu, D. G. Dorrell, L. Alberti, N. Bianchi, D. A. Staton and D. Hawkins

Abstract -- **The paper describes a thermal model for a duplex three–phase induction machine for fault tolerant applications. Three–phase and six–phase variations of duplex three-phase machine operation under fault conditions are considered. Different winding configurations are investigated. Thermal analysis is performed using analytical and finite-element models. Experimental validation is presented for load operating conditions.**

Index Terms-- **AC machines, Thermal conductivity, Motor drives, Dual three phase machines, Fault–tolerant machines, Induction motor, Induction generators, Induction machines, Multiphase machines**

I. Introduction

THE induction machine represents the workhorse of global power conversion; they usually operate as motors but can be used in generating mode. They are relatively cheap and rugged with no brush-gear when the squirrel-cage rotor form is employed. Several of their characteristics are advantageous in electrical drive applications where (in addition to good efficiency) starting, braking, speed reversal and speed change are important. Recently, induction machines have been used in fault tolerant applications [1][2] where multiphase topologies have been adopted. A simple and cost effective solution for multiphase operation is to use multiple sets of three-phase sub-systems. This topology allows industrial "off-the-shelf" three-phase power inverters to be utilized and for redundancy and fault tolerance characteristics to be incorporated. A six-phase machine can realized as a duplex three-phase sub-system, i.e., it can be supplied from one six phase inverter (true six phase) or from two identical three-phase inverters (duplex three-phase). The "multiphase" concept leads to the idea of independent phase sets and fault tolerance so that the machine can continue to operate even when one or more phases have suffered a fault. A multiphase machine is specially designed to have nearly zero magnetic coupling between the sub-systems of three phases, and very low fault current (resulting from high reactance). Generally, for duplex (six-phase) and triplex (nine-phase) machines, the condition to have a low mutual inductance between the sub-systems of three-phases, is to displace them with the electrical angle α so that

$$\alpha = \frac{180\,k}{m} \tag{1}$$

where k is an odd integer ≥ 1 and m is the number of phases. For a six-phase machine we obtain values for the displacement angle between the three-phase sub-systems $\alpha = 30^0$ or 90^0. In Fig. 1, a displacement of 30^0 is shown and this is realised by simple reversing the 3rd and 4th phases in true 6-phase phasor set, as illustrated. If $k = 2$ is used, the displacement angle $\alpha = 60^0$ and the two 3-phase sets that are generated are in anti-phase. This is still a duplex system but with three pairs of phases that are anti-parallel. Again, the phase relationships are shown in Fig. 1 and 3-phase operation is obtained be reversal of the phase winding connections of the second set of windings.

This paper presents the case of duplex three-phase induction motor with anti-phase operation (3-phase) and a displacement angle of 30^0 (6-phase). It is possible to employ various winding configurations for a duplex three-phase induction motor, with different mutual coupling between the two three-phase systems, which affect the rotor currents [1]. The electrical performance of a duplex three-phase system under several fault conditions is investigated in [1].

The aim of this paper is to extend the analysis of the duplex induction-motor to address thermal aspects of operation. A normal operation condition is compared to the open-circuit fault condition. The thermal analysis of the duplex three-phase induction motor is performed using a lumped thermal network and finite-element methods and compared to experimental results.

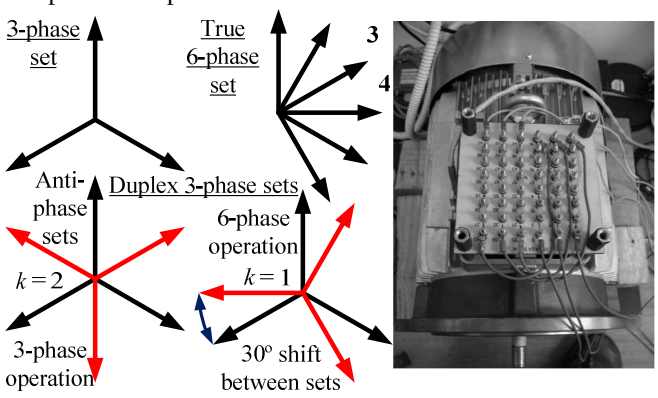

Fig. 1. Phase arrangements and terminal board of tested duplex 3-phase induction machine prototype.

II. Duplex Three-Phase Machine Operation

A prototype duplex three-phase induction motor is shown in Fig. 1. This is a totally enclosed fan-cooled configuration. The motor housing has axial straight distributed fins. All winding coils are connected to a terminal box so that the motor can operate with all possible winding configurations. The general motor data are given in Table I.

A single layer, lap type winding is used to build various configurations that are presented in Fig. 2. Fig. 2(a) shows all the coils. These coils can be used to form a duplex three-phase and six-phase systems from two parallel inverters where k = 1 and $\alpha = 30^0$ or k = 2 and $\alpha = 60^0$; six-phase operation is only achieved using two 3-phase inverters that are out of phase with 30^0 electrical degrees [3]. If the respective inverter phase output voltages are in phase or in anti-phase (where the phase difference is simply corrected by reversing the coil connection) only three-phase operation is possible; this is not six phase operation.

Fig. 2(a) shows the active coils in the machine; i.e. no faults are present. When the machine operates as a three-phase system, each phase has two parallel paths and there are

two coils per pole and per phase. When the machine operates as a six-phase system, there are no parallel paths and just one coil per pole per phase.

TABLE I. Data of the duplex 3-phase induction motor

External diameter D_{ext} [mm]	240
Inner stator diameter D [mm]	150
Stack length L_{stk} [mm]	100
Pole pairs p	4
Stator slots Q_s	48
Rotor slots Q_r	58
Number of turns per coil n_c	60

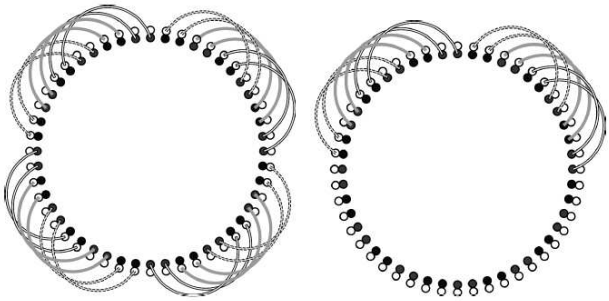

(a) All coils for both 3 and 6-phase windings

(b) Inverter connected coils for 3-phase duplex operation with adjacent series-connected pole-pair windings for one inverter

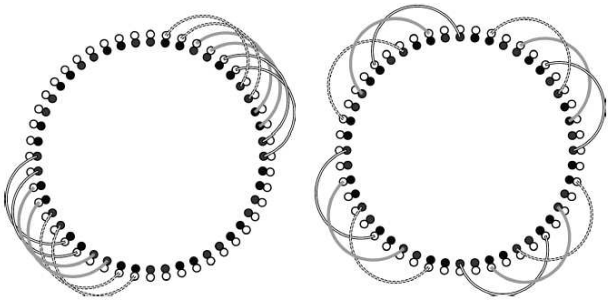

(c) Inverter connected coils for 3-phase duplex operation with opposite series-connected pole-pair windings for one inverter

(d) Inverter connected coils for 6-phase duplex operation with inter-leaved series-connected windings in all poles for one inverter

Fig. 2. Different winding configurations for the duplex connections – (a) all coils in machine; (b)-(d) coils for just one of the inverters.

Fig. 2(b-d) shows winding configurations when the machine operates under fault conditions when only one inverter is active so that only half of the coils are excited. The other coils are open circuited. For the winding configuration in Fig. 2(b) the magnetic and electric loads are concentrated on one half of the machine, hence the losses will be unsymmetrically distributed along the radial periphery of the stator winding. For the winding configurations in Figs. 2(c) and 2(d) there is an electrical and magnetic symmetry of the loading, resulting in a more evenly distribution of the losses.

III. Analytic Thermal Model

The lumped thermal network used to model the duplex three-phase induction motor is described in [8]-[11]. This network uses a layered model, where the copper, insulation and impregnation are evenly distributed through the slot, to produce the equivalent thermal circuit for the winding.

Fig. 3 shows the winding layer model for the analyzed induction machine. This simulation used Motor-Cad design software from Motor Design Ltd [18]. The layered surfaces correlate to the actual areas of the copper, insulation and impregnation. With reference to the thermal model of the analyzed prototype, there are two layers of copper material interlayered with layers of conductor insulation (enamel) and layers of impregnation. The slot liner can be individually defined. The thermal resistances are computed for all the winding components within the slot, Fig. 4 shows the actual location of the conductors within the slot. This illustrates the fill factor.

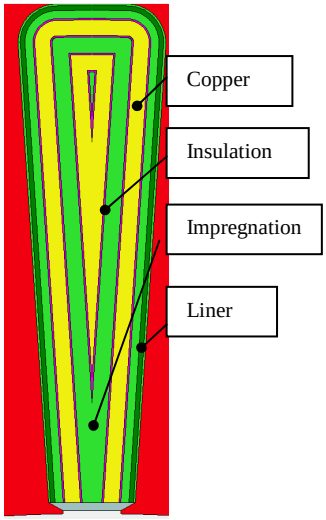

Fig. 3. Conductors layered model of the slot

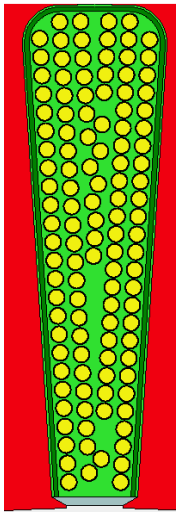

Fig. 4. Conductors random distribution in the slot

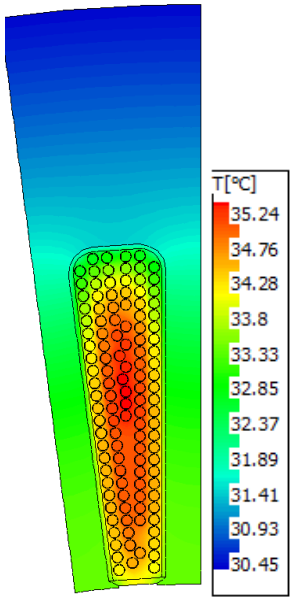

Fig. 5. Temperature distribution within the slot. Normal conditions, only copper losses are considered.

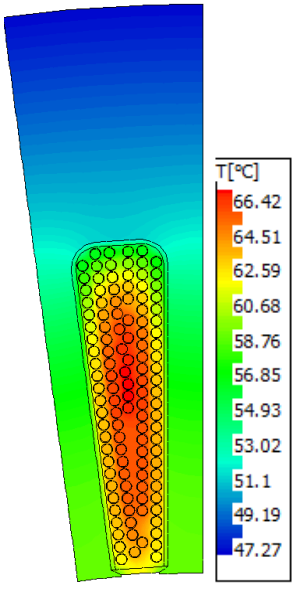

Fig. 6. Temperature distribution within the slot. Faulty conditions, only copper losses are considered.

Figs. 5 and 6 show the temperature distributions in a slot cross-section. These are calculated with a finite-element module, when only the copper losses are considered under normal operation conditions and with fault operation conditions. As expected the maximum temperature spots in the slot are the conductors located along the central axis of the slot, where heat transfer is more difficult. The values of the minimum, average and maximum temperatures in the slot are further used to calibrate the analytical values of the thermal resistances in a model of the slot region.

The motor thermal behavior is simulated using a complex thermal network with 32 nodes. The thermal network nodes shown in Fig. 7 represent the ambient, the stator lamination,

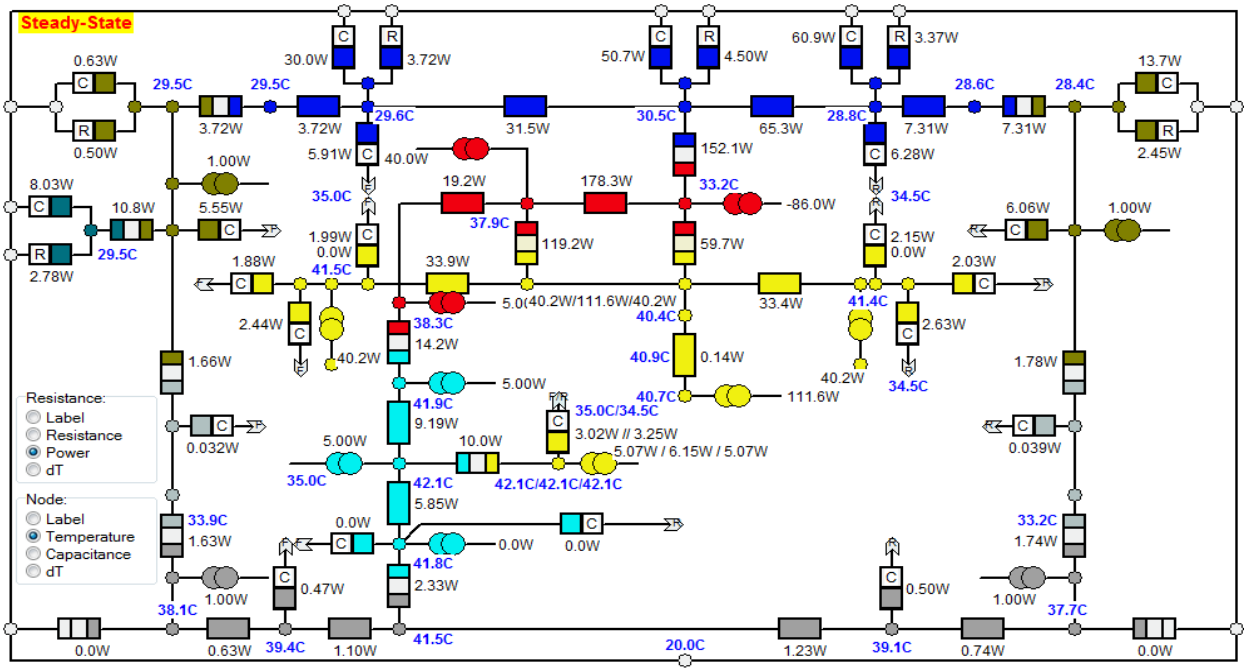

Fig. 7. Thermal network of the duplex 3-phase induction motor.

the housing, the winding and the rotor. The convection and radiation thermal resistances from the housing and end-cap surfaces are calculated using an effective heat transfer coefficient *HTC* (in W/m^2/K) in the model. This is used together with the frame surface area F_{Area} to calculate a frame-to-ambient thermal resistance:

$$R_{FA} = \frac{1}{HTC\ F_{Area}} \tag{2}$$

The calibration of this resistance can account for any fins on the housing by noting that F_{Area} is the effective cylindrical surface area of the frame and end-caps in (2). With such models all the thermal resistances can be calibrated using measurement or more sophisticated thermal models. Another option is to calculate some of the thermal resistances and capacitances based on dimensions and material properties for the particular component. The lumped thermal network provides detailed information for the different heat transfer mechanisms in the machine, i.e., the individual values for convection, radiation, conduction and interface resistances within the geometry can be calculated.

Figs. 8 and 9 show the thermal values distribution at various points in the motor axial and radial sections respectively. Numerical temperatures values at different nodes are given in Table II.

TABLE II. TEMPERATURE VALUES IN VARIOUS NODES OF THE THERMAL NETWORK.

Node Name	Temperature [°C]
Housing	28.2
Rot_Lam_Tooth	38.4
Rot_Lam_Yoke	38.4
Rot_Surface	38.3
Rotor_Bar	38.4
Shaft_Centre	37.9
Stat_Surface	34.3
Stator_Yoke	30.3
ToothMid	33.9
Winding (Average)	36.2
Winding (Maximum)	36.8
Winding (Minimum)	35.9

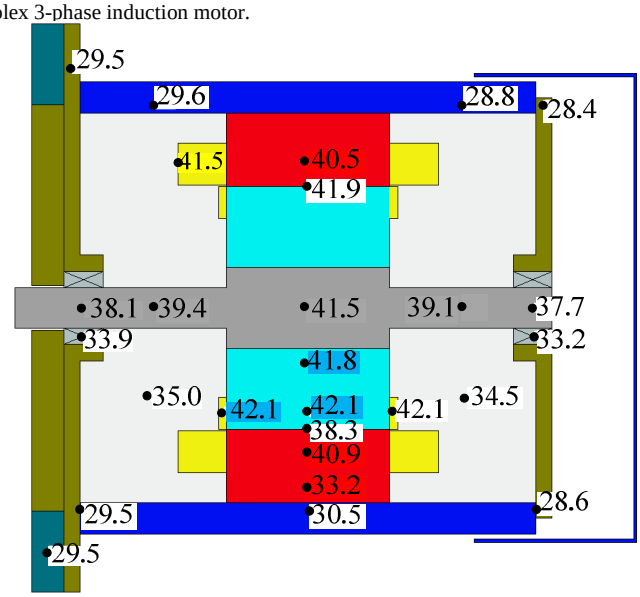

Fig. 8. Thermal values distribution in axial section of the dual 3-phase IM (temperatures in °C).

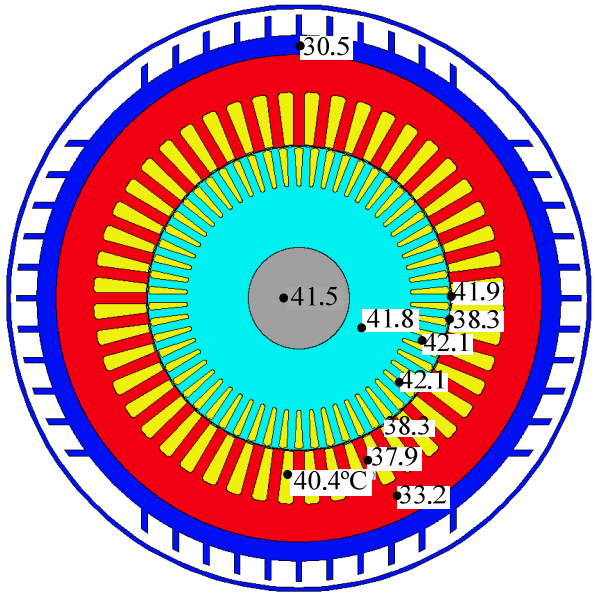

Fig. 9. Thermal values distribution in radial section of the dual 3-phase IM (temperatures in °C).

IV. Finite-Element Thermal Model

The temperature distribution can be calculated using finite-element method. Using a 2D cross-section of the machine, each region – stator and rotor steel, stator winding, rotor cage – is associated with the corresponding material thermal properties; i.e., the thermal conductivity, specific volumetric heat and density. All regions are considered homogenous and isotropic. The various loss components (stator copper loss, rotor cage loss and core loss) are uniformly distributed in the relevant regions. A fixed convection heat transfer coefficient is set on the outer boundary of the stator lamination. The value of the convection heat transfer coefficient is obtained from the analytical thermal lumped model of the machine *HTC* = 55 W/m^2/K (Section III). The most difficult region to model is the stator slot area where the copper conductors are located together with the slot insulation, the conductor insulation and the impregnation material. This problem is solved by using an equivalent thermal conductivity.

A. *Equivalent slot thermal conductivity* [13]

The effective properties of the two dominant isotropic materials in the slot can be used to estimate analytically the equivalent thermal conductivity in the slot using the formulations derived by Hashin [4] or Milton [5]. Hence, the equivalent thermal conductivity of the slot can be calculated using the thermal conductivities of the conductors and the slot impregnation. These are denoted as k_1 and k_2 respectively ($k_1 > k_2$). This approach assumes that the conductor insulation, i.e., the enamel, has the same thermal conductivity as the impregnation material; i.e., a resin type of material. If the conductors are randomly distributed within the slot, and represent f_1 volume ratio of the slot, while the impregnation occupies the volume ratio f_2 (where $f_1 + f_2 = 1$), we can define the equivalent thermal conductivity of the slot as (Hashin [4]):

$$k_e = k_2 \frac{(1+f_1)k_1 + (1-f_1)k_2}{(1-f_1)k_1 + (1+f_1)k_2} \tag{3}$$

Milton [5] proposes two expressions, one for the lower limit of the equivalent property of the two-composite material (k_{eL}) and one the upper limit of the equivalent property (k_{eH}) so that

$$k_{eL} = k_2 \frac{(k_1+k_2)(k_1+k_1f_1+k_2f_2) - f_2\zeta_1(k_1-k_2)^2}{(k_1+k_2)(k_2+k_1f_2+k_2f_1) - f_2\zeta_1(k_1-k_2)^2} \tag{4}$$

$$k_{eH} = k_1 \frac{(k_1+k_2)(k_2+k_1f_1+k_2f_2) - f_1\zeta_2(k_1-k_2)^2}{(k_1+k_2)(k_1+k_1f_2+k_2f_1) - f_1\zeta_2(k_1-k_2)^2} \tag{5}$$

where $\zeta_{1,2}$ represents a general material property calculated by Torquato [6], and tabulated in Table III.

Table III

f_2	0.0	0.1	0.2	0.3	0.4	0.5	0.60
ζ_2	0.0	0.032	0.063	0.092	0.121	0.165	0.251
ζ_1	1.0	0.968	0.937	0.918	0.879	0.835	0.749

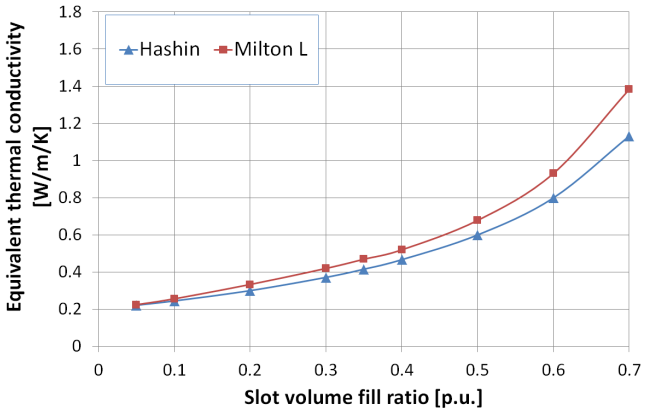

Fig. 10. Slot equivalent thermal conductivity variation with slot volume fill ratio.

For a slot with copper conductors (k_{Cu} = 386W/m/K) and an impregnation resin with k_{Resin} = 0.2W/m/K, the equivalent thermal conductivity of the slot, as calculated using (3) and (4), is plotted in Fig. 10. The prototype duplex three-phase induction machine has a slot fill factor f_1 = 0.4. Hence the slot equivalent thermal conductivity is taken as 0.5 W/m/K. The expression (5) for the upper limit of the equivalent property of the two-composite material was found to lead to substantially higher values and therefore not considered for the estimation of the equivalent thermal conductivity.

B. *Thermal results discussion*

Fig. 11 shows the steady-state temperature isovalues for the normal operation conditions. All slot regions experience a similar temperature gradient as they are subjected to 1/48 of the stator copper loss. The hottest area of the machine is the rotor at 43°C. The average stator winding temperature is estimated to be 37°C. The outer boundary of the stator lamination is predicted to be 34.8°C. The above thermal values are consistent with the analytically determined values in Section III.

Fig. 12 shows the steady-state temperature isovalues under the first case fault conditions (Fig. 2(b)). The stator winding losses are distributed only in the slots located in upper half of the machine. The hottest area of the machine (70°C) corresponds to the coils located in the middle of the energized slots. The machine clearly experiences two different temperature gradients in the two halves of the stator, while the rotor area shows a quasi-uniform temperature of 66°C. This is even though the heat extraction through convection is identical for all the outer boundary of the machine, the temperature distribution is variable. There is almost 20°C temperature difference between the two halves of the machine. Note that the coil conductors that are not energized have a higher temperature than in the case of normal operation conditions with all coils energized; i.e., 53°C against 35°C. This is because the load conditions are set by the voltage and slip; and at the same point, the fault conditions will draw more current from the inverter (about 50 % higher in [1]) while the total motor draws less power. However, here, the current under fault conditions is set to 6 A in the active inverter compared to 5.3 A under normal conditions. The load conditions are given in Table IV. The rotor will have more harmonic MMF waves due to asymmetry so there will be additional rotor losses too.

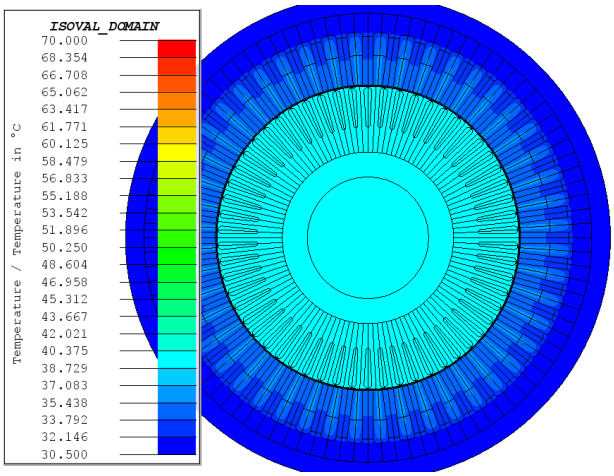

Fig. 11. Temperature isovalues distribution for the duplex 3-phase IM under normal operation conditions.

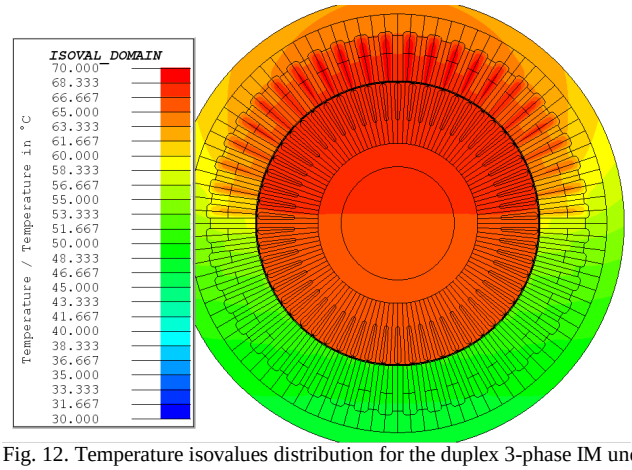

Fig. 12. Temperature isovalues distribution for the duplex 3-phase IM under faulty operation conditions (Fig. 2(b)).

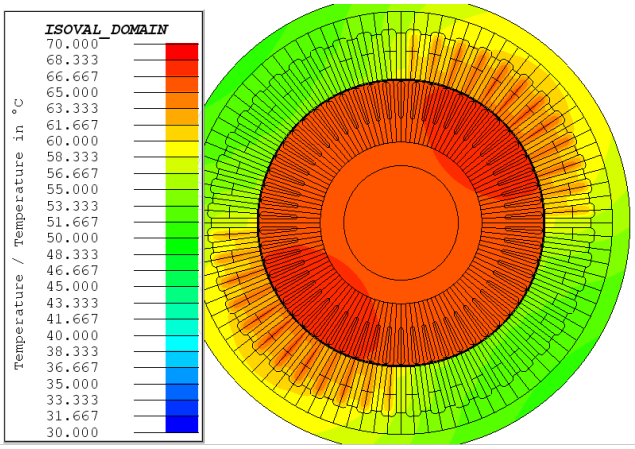

Fig. 13. Temperature isovalues distribution for the duplex 3-phase IM under faulty operation conditions (Fig. 2(c)).

It has to be remembered that the single inverter now has to generate all the magnetic excitation.

Fig. 13 shows the steady-state temperature isovalues under second case fault conditions (Fig. 2(c)). The stator winding losses are distributed only in the slots located in two diametrically opposite quarters of the stator. The hottest area of the machine (66.7°C) is now in the rotor, and this will be due to the additional MMF waves in the rotor. The machine experiences different temperature gradients in each quarter of the stator. The maximum winding temperature is 65°C.

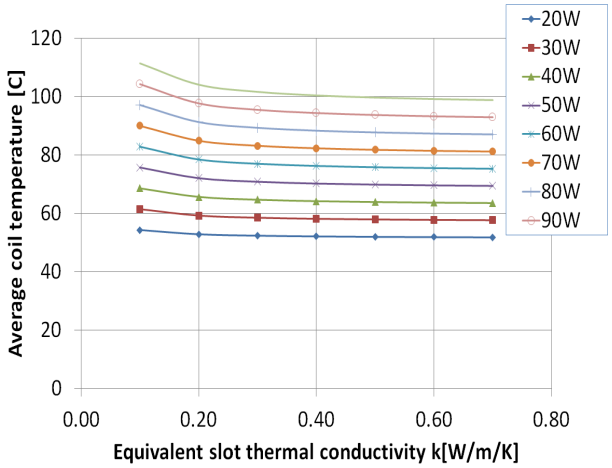

Fig. 14. Average coil temperature [°C] variation with equivalent thermal conductivity (k [W/m/K]) and total copper loss [W]; heat transfer coefficient is assumed to be 55 W/m^2/°C.

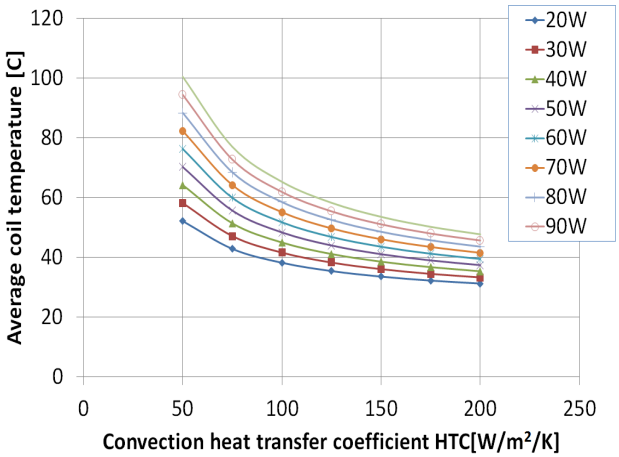

Fig. 15. Average coil temperature [°C] variation with equivalent heat transfer coefficient (HTC [W/m^2/K]) and total copper loss [W]; equivalent slot thermal conductivity is assumed to be 0.5 W/m/K.

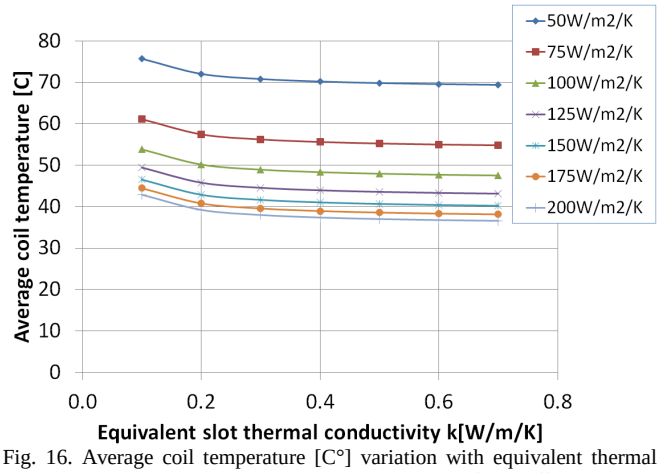

Fig. 16. Average coil temperature [C°] variation with equivalent thermal conductivity (k [W/m/K]) and equivalent heat transfer coefficient (HTC [W/m^2/K]); total copper loss is assumed to be 100 W.

TABLE IV. MEASURED LOSSES (SEE FIG. 2)

	Normal operation	Fault condition (b)	Fault condition (c)
Stator winding loss [W]	50	90	90
Rotor cage loss [W]	15	25	25
Core losses [W]	50	30	30
Current [Arms]	5.3	6.0	6.0

Again, even though the heat extraction through outer-boundary convection is the same around the circumference, the temperature distribution is variable. This time there is

almost 10°C temperature difference between two adjacent quarters of the machine. Similarly to the case in Fig. 12, the coil conductors that are not energized have a higher temperature than in the case of normal operation conditions with all coils energized due to the higher current in the energized coils and current in the rotor; hence 56°C under fault conditions is higher than 35°C.

Fig. 14 presents the sensitivity analysis of the average coil temperature when the slot equivalent thermal conductivity (k) is varied at various values of stator winding copper loss. There is a constant convection heat transfer coefficient of 55 W/m^2/K. Note that for equivalent slot thermal conductivity values that are higher than 0.45W/m/K, which corresponds to a slot fill factor of 0.35, the average coil temperature is practically unchanged for a given loss level.

Fig. 15 illustrates the sensitivity analysis of the average coil temperature when the convection heat transfer coefficient is varied over a range of values for the stator winding copper loss. There is a constant slot equivalent thermal conductivity of 0.5 W/m/K. Note that the winding's average temperature experiences a significant change for a given loss level.

Fig. 16 presents the sensitivity analysis of the average coil temperature when the slot equivalent thermal conductivity (k) changes for various values of the convection heat transfer coefficient while the stator winding copper loss is constant at 100 W. Again there is a greater effect of the convection heat transfer coefficient on the coil temperature.

V. Experimental Results

Three sets of experiments were performed on the duplex three-phase induction motor: on load with normal operation conditions (2 kW output power); with open-circuit fault conditions (the case in Fig. 2(b)) and with half of the winding energized (1 kW output power); and with open-circuit fault conditions (but with the case in Fig. 2(c)) and with two diametrically opposite quarters of the winding energized (1.25 kW output power). The prototype motor was equipped with 12 thermal sensors that were placed as illustrated in Fig. 13: thermal sensor # 1 was placed in slot 48, thermal sensor # 2 was placed in slot 1 and so on. The 12th thermal sensor is located in slot 43. In all cases the machine was supplied with a line voltage of 260 Vrms and 50 Hz frequency. The load was a DC machine acting as a dynamometer. The machine was connected as in Figs. 2(a), (b), and (c). The electromagnetic performance in all cases was reported in [1]. Note that under fault conditions, when only half of the machine was energized, approximately only half of the required mechanical power will be available. As discussed in [1] the configuration in Fig. 2(b) gives a lower output power compared to the configuration in Fig. 2(c).

The segregated measured losses are given in Table IV, while the recorded steady-state temperatures for all 12 sensors are given in Table V.

The measured temperature values show a satisfactory agreement with the calculated values by using a lumped thermal network for the normal operation conditions and finite-element method for the fault conditions.

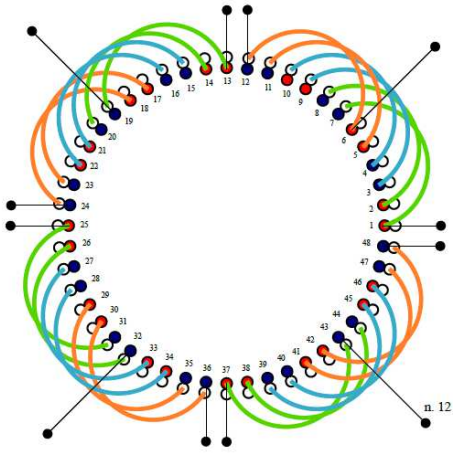

Fig. 17. Thermal sensors placement in the winding; 1st sensor is connected to the conductors in slot 48, 12th sensor is connected to the conductors in slot 43.

These results suggest that at a higher load, under open-circuit fault conditions, all conductors – including those that are not energized – will be subjected to a higher thermal stress than for the normal healthy operation conditions. This phenomenon is valid even though under fault conditions only half output power will be available.

TABLE V. MEASURED STEADY-STATE TEMPERATURES (SEE FIG. 17)

Sensor #	Temperature normal operation [°C]	Temperature fault condition (b) [°C]	Temperature fault condition (c) [°C]
1	35	50	56
2	35	63	66.2
3	35	63	64
4	35	64.4	55
5	35	66.7	54
6	35	62.8	57
7	35	54	64.6
8	35	50	67.4
9	35	50	64
10	35	50	56
11	35	50	54
12	35	53.6	57

VI. Conclusions

A thermal analysis for a duplex three-phase induction motor is presented. Normal operation and fault operating conditions can be accurately modeled using a combination of an analytical lumped thermal network and a finite-element model. The use of an equivalent thermal conductivity for the slot regions to calculate the steady-state temperature distribution is validated through experimental results. Experimental and calculated results show that in open-circuit fault conditions the conductors for the non-energized sub-system will experience higher temperatures compared to the operating temperatures under normal operating conditions, when all sub-systems are energized.

References

[1] L. Alberti and N. Bianchi "Experimental tests of dual three-phase induction motor under faulty operation condition", *IEEE Trans. On Industrial Electronics*, vol. 59, 2012, in press

[2] E. Levi, "Multiphase electric machines for variable-speed applications," *IEEE Transactions on Industrial Electronics*, vol. 55, no. 5, pp. 1893–1909, May 2008.

[3] S. Williamson and A.C. Smith, "Pulsating torque and losses in multiphase induction machines," *IEEE Transactions on Industry Applications*, vol. 39, no. 4, pp. 986–993, Jul./Aug. 2003.

[4] Z. Hashin and S. Shtrikman, "A variational approach to the theory ofthe effective magnetic permeability of multiphase materials," *J. Appl.Phys.*, vol. 33, no. 10, p. 3125, 1962.

[5] G. W. Milton, “Bounds on the transport and optical properties of a two component composite material,” *J. Appl. Phys.*, vol. 52, pp. 5294–5304, 1981.
[6] S. Torquato and F. Lado “Bounds on the conductivity of a random array of cylinders,” *Proc. R. Soc. Lond A*, vol. 417, pp. 59–80, 1988
[7] J. M. Apsley, S. Williamson, A. C. Smith, and M. Barnes “Induction motor performance as a function of phase number,” in *IEE Proceedings Electric Power Applications*, vol. 153, Nov. 2006
[8] D. Staton and M. Popescu, “Analytical thermal models for small induction motors” *COMPEL*, vol. 29, no. 5, 2010, pp. 1345-1360
[9] D. Staton, A. Boglietti, A. Cavagnino, “Solving the More Difficult Aspects of Electric Motor Thermal Analysis, in small and medium size industrial induction motors”, *IEEE Transaction on Energy Conversio*n, Vol.20 (3) pp.620-628.
[10] A. Boglietti, A. Cavagnino, D. Staton, “TEFC Induction Thermal Models: A Parameters Sensitivity Analysis”, *IEEE Transactions on Industry Applications*, Volume 41, Issue 3, May-June 2005, pp. 756 – 763.
[11] D. A. Staton, A. Cavagnino, “Convection Heat Transfer and Flow Calculations Suitable for Electric Machines Thermal Models”, *IEEE Trans. on Industrial Electronics*, Vol. 55, No. 10, October 2008, pp. 3509-3516
[12] L. Alberti and N. Bianchi, “A Coupled Thermal-Electromagnetic Analysis for a Rapid and Accurate Prediction of IM Performance,” *IEEE Transactions on Industrial Electronics*, vol. 55, no. 10, pp. 3575–3582, Oct. 2008.
[13] L. Idoughi, X. Mininger, F. Bouillault, L. Bernard, E. Hoang, “Thermal model with winding homogenization and FIT disrcretization for stator slot” *IEEE Trans. On Magnetics*, Vol. 47, no. 12, December 2011, pp. 4822-4826
[14] M. Popescu “Induction motor modelling for vector control purposes”, Helsinki University of Technology, Report 63, 2000, Espoo
[15] L. Alberti, N. Bianchi, and S. Bolognani, “A Very Rapid Prediction of IM Performance Combining Analytical and Finite-element Analysis,” *IEEE Transactions on Industry Applications*, vol. 44, no. 5, pp. 1505–1512, Sep./Oct. 2008.
[16] R. Kianinezhad, B. Nahid-Mobarakeh, L. Baghli, F. Betin, and G.-A.Capolino, “Modeling and control of six-phase symmetrical induction machine under fault condition due to open phases,” *IEEE Transactions on Industrial Electronics*, vol. 55, no. 5, pp. 1966 – 1977, May 2008.
[17] L. Alberti and N. Bianchi, “Impact of winding arrangement in dual 3-phase induction motor for fault tolerant applications,” in *2010 XIX International Conference on Electrical Machines (ICEM)*, Rome, Italy, 2010, pp. 1 –6.
[18] www.motor-design.com
[19] www.cedrat.com

Mircea Popescu (M’98, SM’04) received the Doctor of Science degree in electrical engineering from Helsinki University of Technology, Finland. He has more than 25 years of experience in electrical motor design and analysis. He worked for the Research Institute for Electrical Machines, Bucharest, Romania, Helsinki University of Technology, Finland and *SPEED* Laboratory, Glasgow University, U.K. Since 2008 he has been the Engineering Manager for Motor Design Ltd., Ellesmere, U.K. He has published over 100 papers in conferences and peer reviewed journals. He is the recipient of the first prize, best paper award from IEEE IAS EMC in 2002, 2006, 2008. He acts as Technical Vice-Chair for ECCE (Energy Conversion Congress and Exhibition) and Vice-Chair of IEEE IAS Electrical Machines Committee.

David George Dorrell (M’95, SM’08) is a native of St Helens, UK, and has a BEng (Hons) degree (1988), MSc degree (1989) and PhD degree (1993). He has held lecturing positions with The Robert Gordon University and The University of Reading. He was a Senior Lecturer with The University of Glasgow, UK, for several years. In 2008 he took up a post with The University of Technology Sydney, Australia, and he was promoted to Associate Professor in 2009. He is also an Adjunct Associate Professor with The National Cheng Kung University, Taiwan. His research interests cover the design and analysis of various electrical machines and also renewable energy systems with over 150 technical publications to his name, including over 50 IEEE Transactions papers and co-authorship of a book on bearingless machines. He is a Chartered Engineer in the UK and a Fellow of the IET. He has sat on IET Council and is active in local area networks. He has acted as a publications chair for IEEE Magnetics Society INTERMAG Conference and also for COMPUMAG. He has also been a guest Editor for the Transactions on Industrial Electronics and is an Associate Editor for the Transactions on Industry Applications. He has won the IEE Cromption Premium in 1996 and two IEEE IAS Electrical Machine Committee prizes. He has carried out consultancy for several electrical machines companies.

Luigi Alberti (S’07, M’09) received the M.S. degree and the PhD in Electrical Engineering from the University of Padova in 2005 and 2009, respectively. He is currently Researcher at the Faculty of Science and Technology of the Free University of Bozen, Italy, working on design, analysis and control of electric machine and drives with particular interest in renewable energy and sustainable mobility.

Nicola Bianchi (M’98, SM’09) received the Laurea and Ph.D. degrees in electrical engineering from the Department of Electrical Engineering, University of Padova, Padova, Italy, in 1991 and 1995, respectively. In 1998, he joined the Department of Electrical Engineering, University of Padova, as an Assistant Professor in electrotechnique. Since 2005, he has been an Associate Professor in electrical machines, converters, and drives. His activity is at the Electric Drives Laboratory, Department of Electrical Engineering, University of Padova. His research activity is in the field of the design of electrical machines, particularly for drive applications. In the same field, he is responsible for various projects for local and foreign industries. He is the author and co-author of several scientific papers on electrical machines and drives and two international books on the same subject. Prof. Bianchi is a member of the IEEE Industry Applications Society (IAS) and the IEEE Power and Energy Society.

David Alan Staton (M’90) received the Ph.D. degree in computer-aided design of electrical machines from Sheffield University, Sheffield, U.K., in 1988. He was with Thorn EMI, the SPEED Laboratory, Glasgow University, U.K., and Control Techniques, U.K., where he worked on motor design and, particularly, the development of motor design software. Since 1999, he has been with Motor Design Ltd., Ellesmere, U.K., which is a new company that he set up to develop thermal analysis software for electrical machines. He has more than 50 papers published in conference proceedings and peer-reviewed journals

Douglas Hawkins received the B.Eng degree in electrical and electronic engineering from the University of Glasgow, U.K. in 1991. From 1991 to 2005 he worked on software control systems on various large projects at GEC Alsthom Traction Ltd., Thomson Marconi Sonar Ltd. and Teleca Ltd. Since 2005 he has been the Software Manager at Motor Design Ltd., Ellesmere, U.K.